Nanosecond Pulsed Plasma Actuators

N. Benard[1], E. Moreau[1], N. Zouzou[1], H. Rabat[2], J. Pons[3], D. Hong[2], A. Leroy-Chesneau[4], P. Peschke[5] and C. Hollenstein[5]

[1] *Pprime,University of Poitiers, CNRS, ISAE-ENSMA, Téléport 2, 86962, Futuroscope, France*
[2] *GREMI, UMR 7344, CNRS, University of Orleans, Orléans, France*
[3] *EPEE FR776, CNRS, University of Orleans Cedex 2, France*
[4] *PRISME, UPRES 4229, University of Orleans, Orléans, France*
[5] *Ecole Polytechnique Fédéral de Lausanne (EPFL), CH-1015 Lausanne, Switzerland*

Abstract

This paper summarizes the results of Plasmaero (EU project) partners on the characterization of plasma actuators based on nanosecond pulsed discharges. Results cover electrical aspects, optical discharge visualizations and measurements of the plasma-induced pressure wave, this for quiescent and transonic flow regimes. Among the results, this study demonstrates that the induced pressure wave is composed of over and under pressure of 1600 and -600 Pa, respectively. In transonic regime, the capability of the discharge to produce a pressure wave remains but this one is convected by the freestream flow.

1 Introduction

The PLASMAERO European project looks at a further understanding of plasma physics for flow manipulation by non-thermal surface discharges. On the margin of typical AC Dielectric Barrier Discharge (DBD) plasma actuators that are based on the produced electric wind [1], different actors of the project are interested in the development of pulsed discharges with rising time in the nanosecond scale order. This type of actuator has demonstrated promising influence to mitigate flow separation at Reynolds numbers related to realistic flight speed conditions [2-4], where AC-DBD have shown only little or no effect. Recent literature suggests that nanosecond pulsed DBD can produce a localized pressure wave that propagates in the medium at speed of sound [5-8] while the induced momentum transfer related to neutral/charged particle collision remains marginal. In the framework of PLASMAERO, different nanosecond pulsed DBDs have been investigated in terms of electrical characteristics for quiescent flow condition. A variety of electrical parameters such as the voltage amplitude, rising time or polarity have been considered. Each partner has used different optical systems that permit detailed qualitative and quantitative descriptions of the propagating pressure waves suspected to be responsible for the control effect and control authority at high speed flow conditions. Later in the project, the behavior of this type of DBD has been investigated in presence of transonic flow. The present paper summarizes the main results obtained in PLASMAERO EU project.

2 Nanosecond pulsed DBD operated in quiescent flow condition

In this first section, different nanosecond pulsed DBD are investigated for initial quiescent flow conditions. As ns-DBD is very flexible, important discharge parameters can be chosen independently. For instance, parameters such as voltage amplitude, rise time or polarity are investigated here.

2.1 Electrical aspects

The electrical measurements for a surface dielectric barrier discharge composed of two electrodes (copper foil with thickness of 40 μm) flush mounted on both sides of a 127 μm thick Kapton layer are shown in figure 1. The gas thermalization at the surface of the dielectric is the result of HV pulse produced by a commercial generator (DEI PVX-4110) connected to a DC power that can supply voltage amplitude up to $\pm$10 kV (Matsuda, 10P30, 30 mA). Results are presented for both positive and negative voltage pulses (absolute voltage amplitudes of 8 and 4 kV, pulse width of 200 ns and rise time about 50 ns).

For a single pulse, two current peaks occur in the total current evolution as shown in Figure 1b. The first one is due to air ionization when the electric field is sufficient to initiate air breakdown. Following the first current peak, charges are deposited at the dielectric surface. When the potential difference between the upper electrode and the charged surface is sufficient, a new discharge propagates on the dielectric. This is verified regardless of the polarity of the HV pulse. The positive voltage pulse presents an asymmetry in the current peak amplitude of the rising and decaying periods. Indeed, a larger amplitude is observed for the primary current peak that results in a significant increase in consumed electrical power (Figure 1c). Opposingly, the amplitude of the current peaks remains of a similar level when DBD is supplied by a negative pulse. Calculation of deposited energy per plasma length indicates that positive HV pulse is more efficient than negative HV pulse, this regardless of the applied voltage amplitude (Figure 1d). As indicated by the discharge current, the first current peak is the main contributor to the energy deposited on the wall surface during an HV pulse. It is suspected that the deposited energy is the key metric for characterizing nanosecond pulsed

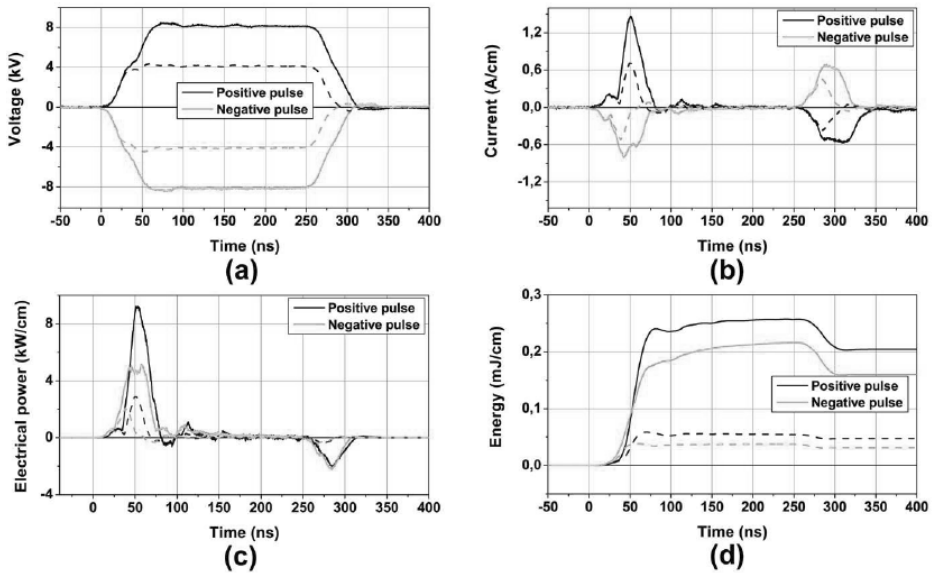

Figure 1: Electrical aspects of positive and negative pulse discharges operated at voltage amplitude of ±8 kV (filled lines) and ±4 kV (dashed lines) with pulse width of 200 ns. (a) Voltage amplitude, (b) Total current (discharge plus displacement currents), (c) Consumed electrical power and (d) Energy deposition

DBD for flow control applications. Indeed, it seems that the pressure wave intensity is directly correlated with the amplitude of the deposited energy [7].

Among the electrical parameters having demonstrated an influence on the pressure wave formation, the rise time of the high voltage pulse is of primary importance as numerically demonstrated by Unfer and Boeuf [9]. Indeed, by reducing the rising time of the input signal, the produced pressure wave should be reinforced by a faster energy deposition into a relatively small volume. The effects of the rising and decaying time are investigated by adding a high voltage resistor in series with the exposed electrode (Figure 2). The amplitude of the signal is adjusted to compensate the voltage drop through the resistor while maintaining a constant output (9.350.15 kV). As illustrated in the figure, the deposited energy reduces in an exponential manner with the time-scale of the rising/decaying period of the voltage signal. By increasing the rising time, tr, by 25 ns from 50 ns, the deposited energy is reduced by 56%. The results indicate that more energy is dissipated, and then potentially converted into gas heating, by reducing the time to attain the maximal (or minimal) voltage amplitude. Furthermore, it was found that a voltage pulse with a steeper slope causes a much shorter and more intense discharge with higher streamer propagation speed. This is illustrated in figure 3, which shows the discharge light emission intensity for two voltage pulses of different rise times tr.

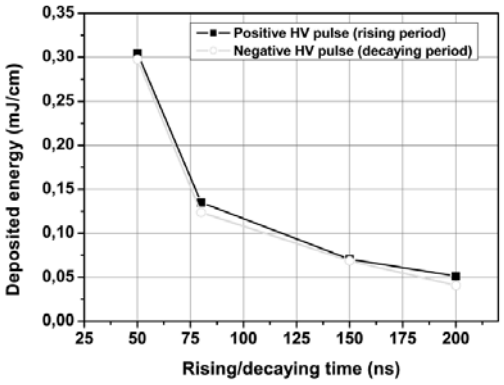

Figure 2: Deposited energy at the dielectric wall according to the rising time (positive high voltage pulse) or decaying time (negative high voltage pulse) for voltage amplitude, U, of ±10 kV

2.2 Plasma morphology

The temporal and spatial discharge development created by the nanosecond pulsed DBD was investigated using ICCD cameras. Measurements are performed for an homebuilt pulse generator constructed using existing power electronics (Mosfet switch). This generator can provide pulse with rise time of a few 10's of nanoseconds, discharge currents up to 30-50 A, frequencies up to 10-20 kHz and voltage amplitude up to 10 kV. In addition, commercial pulse generator is also investigated. This commercial system (described in section 2.1) produces high voltage pulses up to 10 kV amplitude while the rise time is 50 nanoseconds. An illustration of the

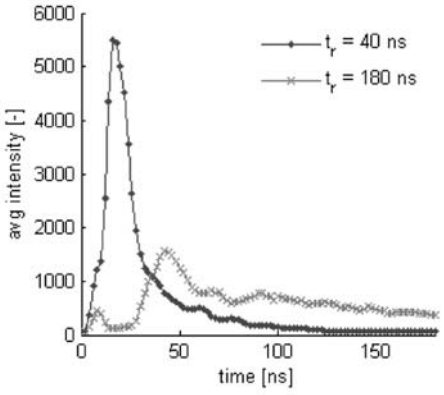

Figure 3: Effect of the rise time on the light emission intensity of a ns-DBD actuator (U = +7 kV)

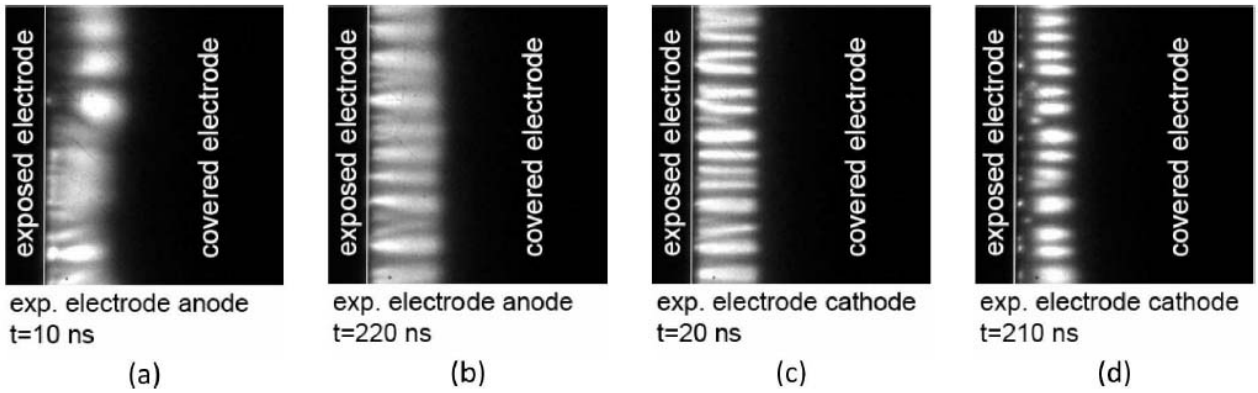

Figure 4: Top-view of the discharge development for homebuilt pulse generator. Cathode directed discharge during voltage rise (a) and fall (b). Anode directed discharge during voltage rise (c) and fall (d)

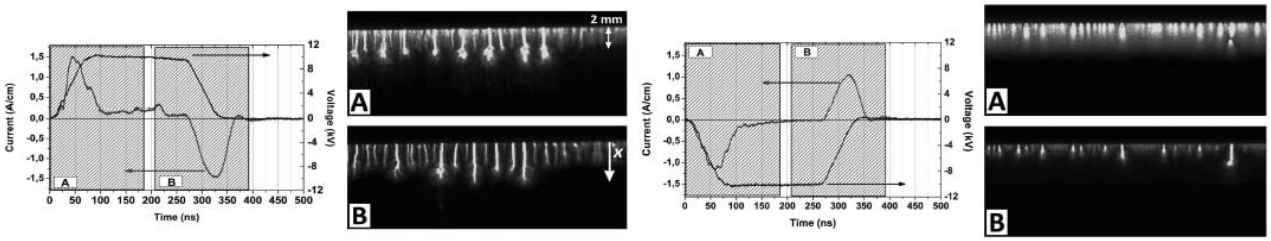

Figure 5: Current evolution and top-view of the discharge development for commercial pulse generator (exposure time of 180 ns). Top figure corresponds to a positive pulse of 10 kV while the bottom plot refers to a negative pulse of -10 kV (pulse width of 200 ns)

plasma discharge obtained by using the homebuilt system is provided in Figure 4. The figure shows the general pattern of the discharge during voltage rise and fall. During voltage rise (Figure 4a), a streamer discharge develops very fast, showing inhomogeneous light emission. The streamers start to develop from the edge of the upper electrode (anode) and propagate along the surface of the dielectric over the lower electrode (cathode). The emission intensity is very high close to the streamer heads. Between these and some bright spots at the edge of the upper electrode, almost no light is emitted. This first discharge is followed by a dark period also referred as "silent period" in [10]. When the voltage pulse ends, a second discharge develops showing a more homogeneous plasma distribution but also a slower propagation speed (Figure 4b). For the negative HV pulse (Figures 4c and 4d), the plasma exhibits an homogeneous pattern made of straight ionization channels.

Typical current evolution and top-view of the gas ionization at the dielectric surface are provided in Figure 5 for DBD actuator supplied by a commercial pulse generator. For the positive HV pulse, the rising and decaying periods produce a filamentary discharge. In its initial stage, the discharge is composed of many streamers distributed along the length of the exposed electrode and superimposed with a corona-like discharge. The straight filaments propagate up to 4 mm, at high speed (0.33 mm/ns in the first instants of the discharge) in the direction of the grounded electrode. During the decaying period of the positive voltage pulse, new plasma forms due to collection of positive charges deposited during the streamer propagation. The plasma is composed again by straight filaments with propagating speed of 0.1 mm/ns. However, the propagation line of the plasma discharge presents a wavy front. This may relate to a non-homogeneous deposition of charged particles at the dielectric wall following the rising period. Nevertheless, the light emitted during the rising voltage period is stronger than the one for the decaying period. This is confirmed by the amplitude of the positive and negative current peaks (1.54 and 1.28 A/cm, respectively).

For the negative HV pulse, the plasma is diffuse and homogeneous along the edge of the active electrode, but some ionization channels are observed. These channels issued from corona spots and propagate with a plume shape that extends up to 2.5 mm. By comparison with a positive high voltage pulse, the filamentary regime, and then occurrence of streamer channels is here significantly reduced. The reduction in streamers results in a shortened discharge propagation that may explain that less energy is deposited on the wall surface.

Finally, the two experiments performed by using two different pulse generators produce differentiated plasma morphology. Results are in agreement when the first discharge is considered. One can say that a streamer discharge develops at voltage rise, while an homogeneous discharge forms at voltage decay. However, the plasma morphology is changed for the discharge related to the second current peak. The difference between the two experiments may result from a larger pulse width with the homebuilt pulse generator that permit a higher relaxation of charged species deposited by the first discharge and then reduce the occurrence of streamers during the voltage decay for positive pulse and voltage rise for negative high voltage pulse.

2.3 Induced pressure wave by nanosecond pulsed DBD

For DBD actuators supplied by high voltage nanosecond pulses, the produced local flow remains weak, subsequently it cannot be considered as the key parameter

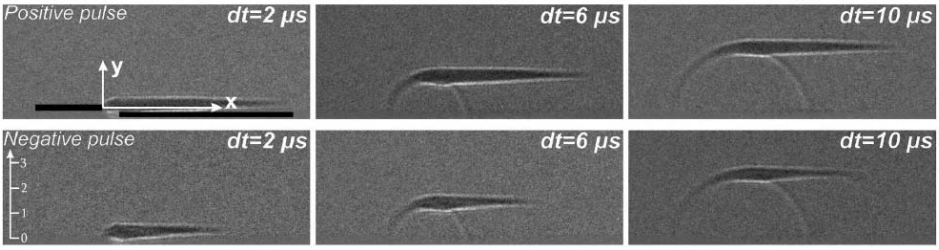

Figure 6: Zoomed visualizations of the propagating pressure wave for positive and negative pulses with width of 200 ns and amplitude of ±10 kV (side view, scale in mm)

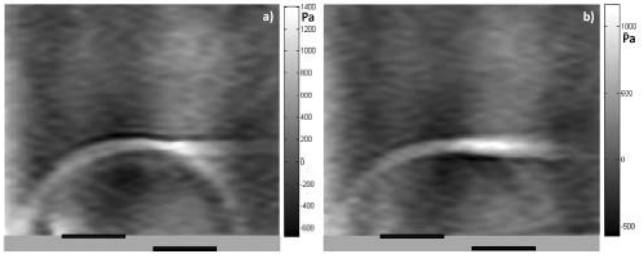

Figure 7: Pressure levels for +15 kV (left) and -15 kV (right) pulses at t = 20 μs

in flow control scenario. As experimentally and numerically demonstrated, pulsed DBD conduces to a rapid energy deposition at the dielectric surface causing a sudden change in the pressure [11, 12]. This abrupt change in the pressure distribution gives rise to a localized pressure wave. It is actually presumed that the mechanism responsible for mitigation or elimination of flow separation is due to the interactions of the pressure wave with coherent flow structures when the wave propagates in the aerodynamic flow. More certainly, such actuator can have particular interest for delaying/promoting laminar-to-turbulent transition. In both cases, the mechanical quantity of primary importance for flow control applications is the produced pressure wave, its intensity and propagation speed. A series of experiments have been conduced to visualize and quantify these pressure waves. They are introduced in this section.

The propagation of the pressure wave produced by the nanosecond pulsed DBD is illustrated in Figure 6 for positive and negative HV pulses (side view). The shadowgraphy images give only qualitative views of the physical phenomenon but they show that the topology of the wave is composed of two distinct parts: A straight region at the top of an hemispheric region. The plate region initiates at the dielectric surface regardless of the pulse polarity. This plate region extends further in the case of a positive HV pulse in agreement with ICCD visualizations. It can be postulated that this part of the pressure wave relates to the streamer developing at the dielectric surface. Calculation of the propagation speed gives a value of 343 m/s, this suggesting that the pressure wave could relate to aeroacoustic noise propagation. This propagation speed is similar for positive and negative pulses of high voltage.

For convenient overpressure field value estimation a time-resolved interferometric imaging setup has been assembled (Mach-Zehnder interferometer). The expanded beam of a 632.8 nm He-Ne laser has been used to produce parallel fringes of equal thickness on a translucent screen at the apparatus outlet. The fringes have been arranged orthogonally to the actuator surface. The cmos sensor (Photron Fastcam SA5 1000K-M2) is used to acquire the interference figure displayed on the screen. When the pressure wave is generated, the consecutive compression or expansion of the air inside the wave front results in refraction index modifications, which appear in the interference figure as fringe distortions. By measuring fringe shifts, $\Delta\varphi$, it is therefore possible to deduce the related index variations, Δn, with the following relation:

$$\Delta n = n - n_0 = \Delta\varphi \times \frac{\lambda}{2\pi L} \tag{1}$$

where n and n_0 are refractive indices of respectively perturbed and unperturbed air (the latter is taken at room temperature), λ the laser wavelength and L the perturbation length. To use this equation it is assumed that the perturbation is independent from the coordinate orthogonal to the picture plane (2D assumption). For an ideal gas the pressure p is related to the refractive index by the Gladstone-Dale equation:

$$n = 1 + \frac{pK}{RT} \tag{2}$$

where K is the Gladstone-Dale constant for the laser wavelength and gas composition of interest, R the ideal gas constant and T the gas temperature. The latter is assumed to be constant and uniform, which is reasonable if dielectric heating consecutive to discharge running can be neglected. Finally, pressure variation can be deduced from phase shift by the following relation:

$$\Delta p = p_0 \times \frac{\Delta\varphi \times \lambda}{(n_0 - 1) \times 2\pi L} \tag{3}$$

Here, the acquisition system is used for an actuator with 100-mm long, 6-mm wide copper electrodes placed at a mutual gap distance of 3 mm on each side of a 0.4-mm thick dielectric (combination of 0.3-mm thick Mylar and two 50 μm thick polyimide layers). The voltage pulse consisted in a nanosecond rise ramp (30 ns) followed by a millisecond range decay [13]. The pulse is obtained by triggering the closure of a fast Thyratron switch (Thyratron Perkin-Elmer HY-3002), in series with the actuator and a capacitor bank. The applied voltage peak value is ±15 kV. The peak power value associated with this pulse is approximately 200 kW, and the corresponding dissipated energy per pulse is close to 0.3 mJ/cm.

According to this processing technique, the overpressure fields have been deduced and results for the two polarities at t = 20 μs are shown in Figure 7. The front shape is similar to those already observed with shadowgraphy (Figure 6) or Schlieren techniques [6]. It shows a pressure excess on one half of the circular part and on the planar part, and a pressure deficit on the second half of the circular part, situated above the plasma. The

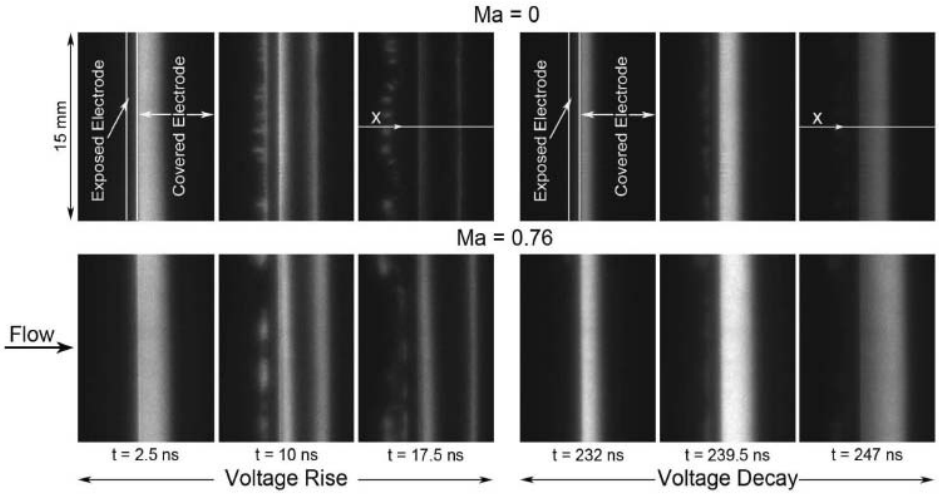

Figure 8: Impact of the flow on the plasma development during voltage rise (left) and fall (right)

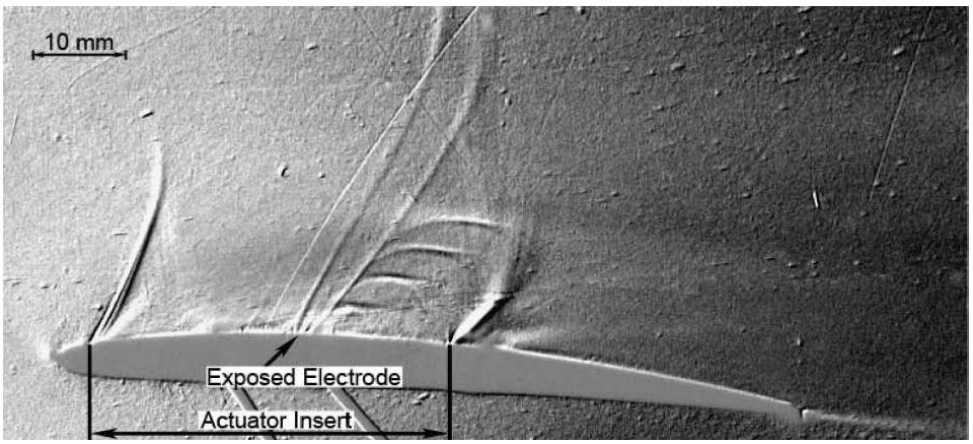

Figure 9: Influence of the flow on the DBD-generated pressure wave ($Ma = 0.76$, $\alpha = 4°$)

maximum pressure is obtained at the junction of cylindrical and planar parts. In the present conditions it is estimated to about 1500 Pa with positive pulse and 600 Pa with negative pulse. The minimum is about -600 Pa for positive pulses, and -200 for negative pulses. It confirms that negative discharges transfer a lower amount of energy to the pressure wave. Values agreeing well with simulations found in the literature [9] even if further setup improvements focusing on increasing phase shifts associated to pressure variations should be done to achieve a better resolution in pressure fields.

3 Nanosecond pulsed DBD operated in situation of transonic flow

Experiments in a transonic wind tunnel have been performed to investigate the characteristics of the ns- DBD in presence of a high speed flow (Ma=0.76). The actuator is integrated on the suction side of a NACA 3506 (span of 40 mm and a length of 77.57 mm).

3.1 Plasma morphology

Phase-averaged images of the discharge development were acquired with a Princeton Instruments PiMax ICCD camera. Figure 8 summarizes the development of the discharge in the absence and presence of flow. An inhomogeneous discharge forms at voltage rise, with a discharge-front that separates from the plasma at the edge of the exposed electrode, whereas a homogeneous discharge is observed at voltage decay, which corresponds to the findings of the experiments without flow. However, the discharge propagation speed, its intensity as well as its extension are increased.

3.2 Induced pressure wave

The propagation of the actuator induced pressure wave was investigated with phase-averaged schlieren images. The behaviour of the ns-DBD generated pressure wave in the presence of flow is shown in figure 9. It is the result of 4 superimposed phase-averaged schlieren images acquired from t = 10 μs to t = 40 μs after the discharge. The shape of this wave is similar to the experiments without flow but it moves downstream with the flow. The propagation speed normal to the DBD surface is still about 330 m/s and the downstream movement of its center corresponds to the flow speed. Due to the highly averaged nature of the schlieren images conclusions of the effect of the actuator on the flow cannot be drawn.

4 Conclusion

The present paper contributes to the body of knowledge on nanosecond pulsed DBD for flow control applications. In particular, it is demonstrated that the actuator can produce a pressure wave presumably useful for flow separation control, this by using different technologies of pulse generators. For the first time, a measure of the pressure level of the induced pressure wave is proposed. Furthermore, it is shown that pressure wave can also be produced in condition of transonic flow regime. However, several partners of the project had to face with difficulties when such actuators are used in wind-tunnel experiments. Indeed, this type of discharge can produce electromagnetic interferences resulting in strong signature of HV pulses in the acquired data or perturbations on the acquisition system.

Acknowledgments

The work has been carried out as a part of PLASMAERO program with funding from the European Community's Seventh Framework Programme FP7/2007-2013 under grant agreement nr. 234201.

References

[1] N. Benard, E. Moreau, 2012, *EHD Force and Electric Wind Produced by Plasma Actuators Used for Airflow Control*, AIAA paper 2012-3136.

[2] D. Roupassov, A. Nikipelov, M. Nudnova, and A. Starikovskii, 2009, *Flow separation control by plasma actuator with nanosecond pulsed-periodic discharge*, AIAA J., Vol. 47, pp. 168-185.

[3] J. Little, K. Takashima, M. Nishihara, I. Adamovich, and M. Samimy, 2012, *Separation Control with Nanosecond-Pulse-Driven Dielectric Barrier Discharge Plasma Actuators,* AIAA J., Vol. 50, pp. 350-365.

[4] S.M. Aulchenko, V.P. Zamuraev, and A.P. Kalinina, 2009, *Control of the aerodynamic characteristics of wing airfoils by nonstationary energy supply in transonic flow*, J. Engineering Physics and Thermophys., Vol. 82, pp. 16, 20.

[5] I.A. Znamenskaya, D.F. Latfullin, A.E. Lutskii, and I.V. Musenkova, 2010, *Energy deposition in boundary gas layer during initiation of nanosecond sliding surface discharge*, Techn. Phys. Letters, Vol. 36, pp. 795-797.

[6] K. Takashima, Y. Zuzeek, W.R. Lempert, and I.V. Adamovich, 2011, *Characterization of surface dielectric barrier discharge plasma sustained by repetitive nanosecond pulses*, Plasma Source Sci. Technol., Vol. 20, pp. 055009.

[7] N. Benard, N. Zouzou, A. Claverie, J. Sotton, and E. Moreau, 2012, *Optical visualization and electrical characterization of fast-rising pulsed dielectric barrier discharge for airflow control applications,* J. Applied Physics, Vol. 111, 033303.

[8] J. Little, and R. Dawson, 2012, *Characterization of Nanosecond Pulse Driven Dielectric Barrier Discharge Plasma Actuators for Aerodynamic Flow Control*, AIAA paper 2012-188

[9] T. Unfer, and J.P. Boeuf, 2010, *Modeling and comparison of sinusoidal and nanosecond pulsed surface dielectric barrier discharges for flow control*, Plasma Phys. Control. Fusion, Vol. 52, pp. 124019.

[10] A.Y. Starikovskii, A.A. Nikipelov, M.M. Nudnova, M.M., and D.V. Roupassov, 2009, *SDBD plasma actuator with nanosecond pulse-periodic discharge*, Plasma Sources Sci. Technol., Vol. 18, pp. 034015.

[11] I.A. Znamenskaya, D.F. Latfullin, A.E. Lutskii, A.E., and I.V. Musenkova, 2010, *Energy deposition in boundary gas layer during initiation of nanosecond sliding surface discharge*, Techn. Phys. Letters, Vol. 36, pp. 795-797.

[12] T. Unfer, and J.P. Boeuf, 2009, *Modelling of a nanosecond surface discharge actuator*, J. Physics D Applied Physics, Vol.42, pp.194017.

[13] H. Rabat, J. Pons, D. Hong, and A. Leroy, 2011, *Study of an atmospheric surface barrier discharge actuator using a nanosecond rising high-voltage power supply*, Proc. 20th Int. Symp. in Plasma Chem., Philadelphia, USA, July 24-29, 2011.